

## Local transport in a disorder-stabilized correlated insulating phase

M. Baenninger, A. Ghosh, M. Pepper, H. E. Beere, I. Farrer, P. Atkinson, and D. A. Ritchie  
*Cavendish Laboratory, University of Cambridge, Madingley Road, Cambridge CB3 0HE, United Kingdom*  
 (Received 13 October 2005; published 22 December 2005)

We report the experimental realization of a correlated insulating phase in two-dimensional (2D) GaAs/AlGaAs heterostructures at low electron densities in a limited window of background disorder. This has been achieved at mesoscopic length scales, where the insulating phase is characterized by a universal hopping transport mechanism. Transport in this regime is determined only by the average electron separation, independent of the topology of background disorder. We have discussed this observation in terms of a pinned electron solid ground state, stabilized by the mutual interplay of disorder and Coulomb interaction.

DOI: [10.1103/PhysRevB.72.241311](https://doi.org/10.1103/PhysRevB.72.241311)

PACS number(s): 73.21.-b, 73.20.Qt

In the presence of Coulomb interaction, both magnetic field and disorder are predicted to stabilize many-body charge-ordered ground states.<sup>1,2</sup> Strong perpendicular magnetic field  $B_{\perp}$  quenches the vibrational motion of electrons, and has been extensively exploited to realize a charge-density wave (CDW) ground state in systems with weak background disorder.<sup>3,4</sup> Despite the effort, however, the nature of localization in such systems has been controversial, with both pinned Wigner solid (WS) formation and inhomogeneity driven percolation transition being suggested.<sup>5</sup> On the other hand, disorder stabilizes Coulomb correlation effects by introducing a pinning gap  $\Delta_{\text{pin}}$  in the phonon density of states, which provides a long-wavelength cutoff.<sup>2</sup> This has led to the theoretical prediction of several forms of CDW ground states at zero or low  $B_{\perp}$ . Systematic experimental investigations on such possibilities, however, have been rare, and form the subject of this work.

Increasing the magnitude of background potential fluctuations increases  $\Delta_{\text{pin}}$ , which stabilizes the CDW phases to higher temperatures. In modulation-doped GaAs/AlGaAs heterostructures, where disorder primarily arises from the charged dopant ions,<sup>6</sup>  $\Delta_{\text{pin}} \sim \exp(-4\pi\delta_{\text{sp}}/\sqrt{3}r_{\text{ee}})$  depends strongly on the setback distance  $\delta_{\text{sp}}$  that separates the 2D electron system (2DES) and the dopants, where  $r_{\text{ee}}$  is the mean distance between the electrons in the 2DES (Refs. 7 and 8). However, disorder affects the ground-state transport in two critical ways. First, the presence of  $\Delta_{\text{pin}}$  disintegrates the CDW phase into domains of finite size  $\lambda_d \sim \text{sound velocity}/\Delta_{\text{pin}}$ . At strong pinning,  $\lambda_d$  becomes microscopically small, leading to significant averaging in transport measurements with conventional macroscopic devices. Second, strong potential fluctuations can also result in a “freezing” of transport below a certain percolation threshold even when electron density ( $n_s$ ) is relatively high, thereby making the regime of strong effective Coulomb interaction inaccessible.

Here, we show that these difficulties can be largely overcome by using modulation-doped heterostructures of mesoscopic dimensions. In such devices transport freezes at much lower  $n_s$  in comparison to macroscopic devices at the same  $\delta_{\text{sp}}$  or disorder, thereby allowing transport at a large interaction parameter  $r_s = 1/a_B^* \sqrt{\pi n_s} \sim 7-8$  ( $a_B^*$  is the effective Bohr radius), even when  $\delta_{\text{sp}}$  is relatively small. The typical dimen-

sion  $L$  of our devices in the current carrying direction was chosen to be  $\sim 2-4 \mu\text{m}$ , which is also similar in order of magnitude to the  $\lambda_d$  suggested by recent microwave absorption studies for pinned WS ground states.<sup>4</sup> The low- $B_{\perp}$  magnetotransport in these devices was found to display a striking universality in that the hopping distance in the localized regime was determined by  $r_{\text{ee}} = 1/\sqrt{n_s}$ , rather than the details of background disorder, indicating an unusual self-localization of electrons at sufficiently low  $n_s$ .

We have used Si modulation-doped GaAs/AlGaAs heterostructures where  $\delta_{\text{sp}}$  was varied from 20 to 80 nm. At a fixed  $n_s$ , the effect of  $\delta_{\text{sp}}$  on the strength of potential fluctuations is reflected in the mobility  $\mu$ , as can be observed from Fig. 1(b). Both monolayer ( $\delta$ )- and bulk-doped wafers were used. Relevant properties of the devices are given in Table I. Devices were cooled from room temperature to 4.2 K over 24–36 h to allow maximal correlation in the dopant layer [redistribution of charged-donor ( $DX$ ) centers].<sup>9</sup> This slow cooldown technique also leads to excellent reproducibility over repeated thermal cycles. Electrical measurements were carried out with a standard low-frequency (7.2 Hz) four-probe technique with an excitation current of  $\sim 0.01-0.1$  nA to minimize heating and other nonlinear effects. A direct measurement of  $n_s$  within the mesoscopic region was carried out with an edge-state reflection-based technique.<sup>10</sup>

In Fig. 1(a) we compare the  $n_s$  scale of localization transition at  $B_{\perp} = 0$  and  $T = 0.3$  K in macroscopic and mesoscopic devices from the same wafer. In a standard  $100 \times 900 \mu\text{m}^2$  Hall bar, as illustrated with wafer A2677, the linear conductivity  $\sigma \rightarrow 0$  [A77L, inset of Fig. 1(a)] at  $\sim 3$  times the  $n_s$  compared to the mesoscopic sample (A77) from the same wafer. Further,  $\sigma$  in the large sample A77L shows excellent classical percolationlike scaling  $\sigma \sim (n_s - n_c)^\gamma$  ( $n_c = 1.72 \times 10^{10} \text{ cm}^{-2}$ ), where  $\gamma \approx 2$ , implying a inhomogeneity driven percolation transition at nonzero  $T^5$  [solid line in the inset of Fig. 1(a)]. Similar scaling in the mesoscopic systems, however, was found to be difficult, with unphysically large estimates of  $\gamma \sim 3.2-3.7$  (not shown), indicating a different mechanism of localization transition.

As  $n_s$  is lowered below a sample-dependent characteristic scale  $n_s^*$  [denoted by the crosses in Fig. 1(a)], the onset of strong localization is identified by the resistivity  $\rho (=1/\sigma)$  exceeding  $\approx h/e^2$ . At  $n_s \ll n_s^*$ , the  $T$  dependence of  $\rho$  at a

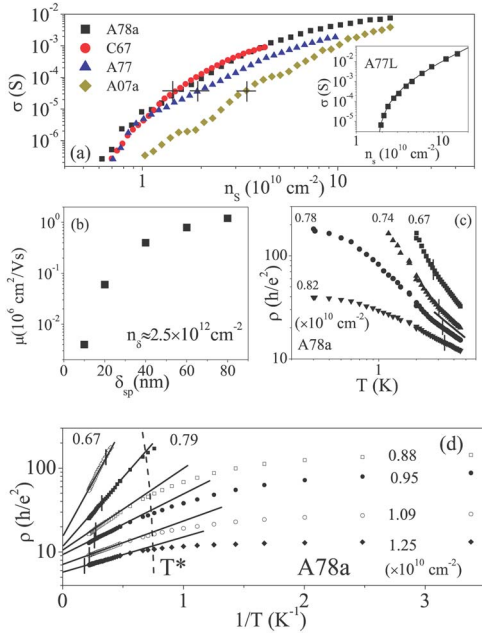


FIG. 1. (Color online) (a) Conductivity ( $\sigma$ ) of mesoscopic samples as a function of electron density  $n_s$  at  $T \approx 0.3$  K. The crosses denote  $n_s^*$  for individual samples (see text). Inset:  $n_s$  dependence of  $\sigma$  for a macroscopic Hall bar A77L. The solid line is the best fit of a classical percolationlike scaling relation  $\sigma \sim (n_s - n_c)^\gamma$ . (b)  $\delta_{sp}$  dependence of mobility at constant  $n_s$  and  $n_\delta$  for heterostructures similar to those used in presented work. (c) Resistivity ( $\rho$ ) as a function of temperature measured at  $B_\perp = 1$  T. The solid line represents a power law of  $\sim T^{-1}$ ; the vertical lines in (c) and (d) indicate the Fermi temperatures  $T_F$ . (d) Activation and saturation of  $\rho$  at  $B_\perp = 1.5$  T.

fixed  $n_s$  can be divided into three regimes, as illustrated with A78a: First, transport in the classical regime at  $T \geq T_F$  is magnified in Fig. 1(c), where  $T_F$  is the Fermi temperature. In this regime  $\rho \propto T^{-\beta}$ , where  $\beta \sim 1$  (indicated by the solid line). As  $T$  is decreased, the onset of the quantum regime ( $T \lesssim T_F$ ) results in a stronger increase in  $\rho$  with decreasing  $T$ . Note that the clear classical to quantum crossover implies a

TABLE I. Geometrical and structural property of the devices.  $n_\delta$  is the density of Si dopants and  $W$  is the width. The background doping concentration is  $\leq 10^{14}$  cm $^{-3}$  in all devices.

Wafer	Device	$\delta_{sp}$ (nm)	$n_\delta$ ( $10^{12}$ cm $^{-2}$ )	$W \times L$ ( $\mu\text{m} \times \mu\text{m}$ )	Doping
A2407	A07a	20	2.5	$8 \times 2$	$\delta$
	A07b	20	2.5	$8 \times 3$	$\delta$
A2678	A78a	40	2.5	$8 \times 2.5$	$\delta$
	A78b	40	2.5	$8 \times 4$	$\delta$
A2677	A77	40	— <sup>a</sup>	$8 \times 3$	Bulk
	A77L	40	— <sup>a</sup>	$100 \times 900$	Bulk
C2367	C67	60	0.7	$8 \times 3$	$\delta$
T546	T46	80	1.9	$8 \times 3$	$\delta$

<sup>a</sup>The doping concentration of bulk-doped devices is  $2 \times 10^{18}$  cm $^{-3}$  over a range of 40 nm.

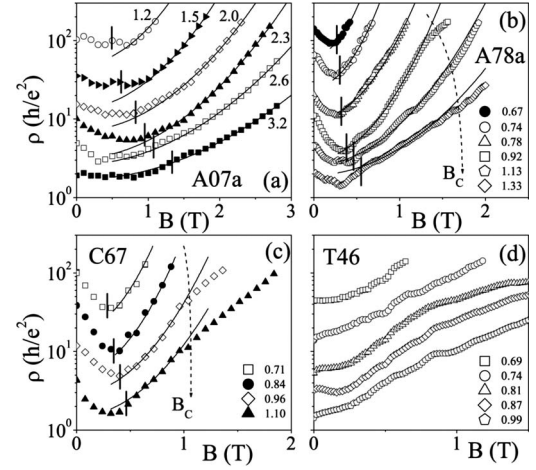


FIG. 2. Typical magnetoresistivity traces in four samples with varying levels of disorder. The vertical lines denote  $\nu=1$ . The numbers indicate electron density in units of  $10^{10}$  cm $^{-2}$ .  $B_c$  denotes the field scale up to which a quadratic  $B_\perp$  dependence could be observed. The parameters  $\alpha$  and  $\rho_B$  were obtained from the slope and  $y$  intercept of linear fits to  $\ln(\rho) - B_\perp^2$  traces, respectively.

well-defined  $T_F$ , and hence a uniform charge-density distribution down to the lowest  $n_s \sim 6.5 \times 10^9$  cm $^{-2}$  (in A77L, inhomogeneity sets in at  $n_s$  as large as  $\sim 4-5 \times 10^{10}$  cm $^{-2}$ ). In the quantum regime and for  $T_F > T > T^*$ , Fig. 1(d) shows that the behavior of  $\rho$  is activated with  $\rho(T) = \rho_3 \exp(\epsilon_3/k_B T)$ , where  $\epsilon_3$  is the activation energy. From the  $n_s$  and  $B_\perp$  dependence of the pre-exponential  $\rho_3$ , we have shown earlier that the transport mechanism in this regime corresponds to nearest-neighbor hopping.<sup>10</sup> Below the characteristic scale  $T^* \sim 1$  K, variation of  $\rho$  becomes weak, tending to a finite magnitude even in the strongly localized regime. This saturation in the insulating regime cannot be explained in terms of an elevated electron temperature due to insufficient thermal coupling to the lattice since  $T^*$  depends only weakly on electron density up to  $n_s \sim n_s^*$  [Fig. 1(d)], and the damping of Shubnikov-de Haas oscillations in the metallic regime shows the base electron temperature to be  $\approx 300$  mK.

In order to explore the physical mechanism behind the weak  $T$  dependence of  $\rho$ , we have carried out extensive magnetoresistivity (MR) measurements at the base  $T$ . Figures 2(a)–2(d) show the  $B_\perp$  dependence of MR in the insulating regime of four devices with increasing  $\delta_{sp}$  from 20 to 80 nm. In general, we find a strong negative MR in A07, A78, and C67 at low  $B_\perp$ , which can be attributed to interference of hopping paths. The negative MR is followed by an exponential rise in  $\rho$  as  $B_\perp$  is increased further. We have recently shown that the logarithm of such a positive MR at low  $B_\perp$  varies in a quadratic manner with  $B_\perp$ , i.e.,  $\rho(B_\perp) = \rho_B \exp(\alpha B_\perp^2)$ , where  $\rho_B$  and  $\alpha$  are  $n_s$ -dependent factors.<sup>10</sup> Such a variation, denoted by the solid lines in Fig. 2, is found to be limited to  $n_s \leq n_s^*$ , and extends over a  $B_\perp$  scale of  $B_c$ , where  $B_c$  was found to decrease rapidly as  $\delta_{sp}$  is increased. Note that in T46 (lowest disorder), neither a clear negative MR nor an exponential  $B_\perp^2$  dependence were observed. A physical significance of  $B_c$  and of the qualitatively different MR behavior of T46 will be discussed later.

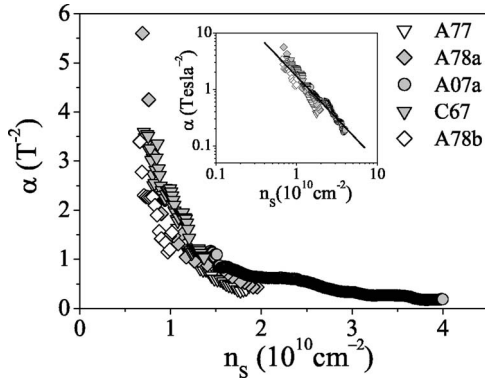


FIG. 3. Absolute magnitude of  $\alpha$  obtained from the slope of  $\ln(\rho) - B_{\perp}^2$  traces for five different samples. The inset shows the same data in a log-log scale. The slope of the solid line is  $-3/2$ .

The observed behavior of  $\rho$  can be naturally explained in the framework of tunneling of electrons between two trap sites separated by a distance  $r_{ij}$ . In weak  $B_{\perp}$ , such that the magnetic length  $\lambda = \sqrt{\hbar/eB_{\perp}} \gg \xi$ , where  $\xi$  is the localization length, the asymptotic form of the hydrogenic wave function changes from  $\psi(r) \sim \exp(-r/\xi)$  to  $\psi(r) \sim \exp(-r/\xi - r^3\xi/24\lambda^4)$ . (Ref. 11). This leads to a MR,  $\rho(B_{\perp}) = \rho_0 \exp(2r_{ij}/\xi) \exp(Ce^2 r_{ij}^3 \xi B_{\perp}^2 / 12\hbar^2)$ , which implies

$$\rho_B = \rho_0 \exp(2r_{ij}/\xi) \text{ and } \alpha = Ce^2 r_{ij}^3 \xi / 12\hbar^2. \quad (1)$$

While  $\rho_B$  depends on the tunneling probability at  $B_{\perp}=0$ ,  $\alpha$  denotes the rate of change of this probability when  $B_{\perp}$  is switched on. Importantly, both parameters provide information on the intersite distance  $r_{ij}$ , as well as  $\xi$  independently. The parameter  $C \sim 0.5 - 1$  depends on the number of bonds at percolation threshold in the random resistor network (we shall subsequently assume  $C \approx 1$ ). Since conventional hopping sites are essentially impurity states, both  $\alpha$  and  $\rho_B$  are expected to be strongly disorder dependent. Note that, since wave-function overlap plays a critical role in transport, a direct source-to-drain tunneling is ruled out in our case.<sup>12</sup>

From the MR data we have evaluated  $\alpha$  and  $\rho_B$  from the slope and intercept of the  $\ln(\rho) - B_{\perp}^2$  traces. Further details of the analysis can be found elsewhere.<sup>10</sup> In Fig. 3 we have shown  $\alpha$  as a function of  $n_s$  for five different samples up to the corresponding  $n_s^*$ . Strikingly, the absolute magnitudes of  $\alpha$  from different samples are strongly correlated, and can be described by a universal  $n_s$ -dependent function over nearly two orders of magnitude. At stronger disorder (e.g., A07), localization occurs at a higher  $n_s$  resulting in a lower  $\alpha$ , while at lower disorder (e.g., C67) localization occurs at lower  $n_s$ , yielding a larger magnitude of  $\alpha$ . This indicates that magnetotransport in such mesoscopic samples is not determined directly by disorder, but by  $n_s$  in the localized regime. Qualitatively, the decreasing behavior of  $\alpha$  with increasing  $n_s$  itself is inconsistent with the single-particle localization in an Anderson insulator.<sup>10,13</sup>

From the strong sample-to-sample correlation in the magnitude of  $\alpha$ , a disorder-associated origin of  $r_{ij}$  is clearly unlikely. For example, taking  $r_{ij} \sim \delta_{sp}$  will lead to distinct sets of  $\alpha$  for wafers with different  $\delta_{sp}$ . However, in the context of

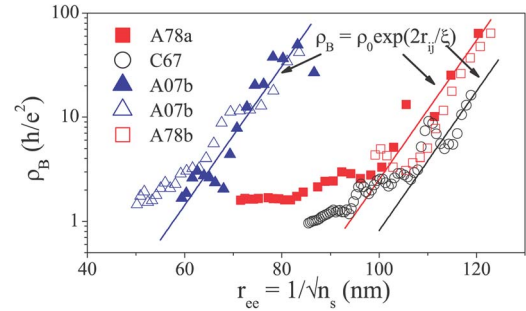


FIG. 4. (Color online) The dependence of  $\rho_B$  on the average electron separation  $r_{ee}$  in five different samples. The slope of the solid lines gives an estimate of  $\xi$  [Eq. (1)].

a pinned CDW ground state, another relevant length scale is  $r_{ee}$ . Indeed, in a case of tunneling events over a mean electron separation, i.e.,  $r_{ij} \approx r_{ee}$ , we find that Eq. (1) describes both absolute magnitude, as well as the  $n_s$  dependence of  $\alpha$  quantitatively. Using  $r_{ij} \approx 1/\sqrt{n_s}$ , Eq. (1) leads to  $\alpha \propto n_s^{-3/2}$ , as indeed observed experimentally (solid line in the inset of Fig. 3). Allowing for sample-to-sample variation, we find  $\alpha = (1.7 \pm 0.5) \times 10^{21} / n_s^{3/2} T^{-2}$  from which, using Eq. (1), we get  $\xi = 9.0 \pm 2.6$  nm, which is close to  $a_B^*$  in GaAs ( $\approx 10.5$  nm).

The analysis can be immediately checked for consistency from the  $r_{ee}$  dependence of  $\rho_B$ . From Fig. 4, we find that  $\rho_B$  increases strongly with increasing  $r_{ee}$  when  $n_s \ll n_s^*$ , as expected in the simple tunneling framework [Eq. (1)]. In spite of the scatter, the overall slopes of the  $\ln(\rho_B) - r_{ee}$  plots are similar in different samples (solid lines) with  $\xi$  estimated to be  $\approx 13 \pm 4$  nm, agreeing with that obtained from the analysis of  $\alpha$ . Note that the  $\rho_B$  deviates from the exponential dependence and tends to saturate as  $n_s \rightarrow n_s^*$ . While this is not completely understood at present, we note that the saturation in  $\rho_B$  occurs within the range  $\rho_B \sim 1 - 2 \times h/e^2$ , irrespective of sample details. Similar universality in the hopping pre-exponential has been observed in the context of  $T$  dependence of  $\rho$  in variable-range hopping,<sup>14</sup> and has been suggested to indicate an electron-electron interaction mediated energy-transfer mechanism.

We now discuss the physical scenario which could lead to the electron separation-dependent hopping transport. We show that our observations can be explained in the theoretical framework of defect motion in a quantum solid that was originally developed by Andreev and Lifshitz in the context of solid He<sup>3</sup> (Ref. 15), and later adapted for a WS ground state.<sup>16,17</sup> In our case, transport in both the quantum and classical regime can be understood in terms of tunneling of localized defects in an interaction-induced pinned electron solid phase as  $n_s$  is reduced below the melting point  $n_s^*$ . The defects, which act as quasiparticles at low  $T$ , can arise from regular interstitials, vacancies, dislocation loops, etc., as well as from zero-point vibration of individual lattice sites.<sup>15</sup> The scale of zero-point fluctuation  $\sim \hbar / r_{ee} \sqrt{m^* U_C} \approx 2\pi / \sqrt{r_s} \gg 1$ , is indeed strong in our case over the experimental range of  $n_s$ , where  $U_C \approx e^2 / 4\pi\epsilon r_{ee}$  is the interatomic interaction energy scale.

In the quantum regime, the transport at higher  $T$  ( $T_F \gg T \gg T^*$ ) is predicted to be thermally activated nearest-neighbor

hopping of localized defects, while at lower  $T(\ll T^*)$  tunneling of such defects leads to a  $T$ -independent transport.<sup>15</sup> While this clearly describes the weak  $T$  dependence of  $\rho$  at low temperatures [Fig. 1(d)], the strongest support of this picture comes from the fact that the natural length scale of tunneling is indeed the average electron separation  $r_{ee}$ . This immediately explains the unusual  $n_s$  (or  $r_{ee}$ ) dependence of both  $\alpha$  and  $\rho_B$ , as well as the apparent insensitivity of these parameters to local disorder. The negative MR at low  $B_\perp$  caused by destruction of interference is then expected to persist up to a  $B_\perp$  corresponding to  $\nu = n_s h/eB_\perp \sim 1$  (one flux quantum  $\phi_0$  within an area of  $r_{ee}^2$ ), as indeed observed in our experiments (Fig. 2). The tunneling of a defect scenario also allows an estimate of the crossover scale  $k_B T^* = \epsilon_3 / \ln(\Delta_{\text{pin}}/\Delta\epsilon)$  (Ref. 15), where  $\Delta\epsilon$  is the bandwidth. For a pinned WS ground state, using the expression of  $\Delta_{\text{pin}}$  in Ref. 8, experimentally measured  $\epsilon_3$ , and  $\Delta\epsilon \sim h^2/8m^*r_{ee}^2$ , we find  $T^* \sim O(1 \text{ K})$  over the experimental range of  $n_s$  in A78a, giving good order-of-magnitude agreement to the observed scale of  $T^*$ . Finally, the behavior of  $\rho \sim T^{-1}$  in the classical regime ( $T > T_F$ ) [Fig. 1(c)] has also been recently observed,<sup>18</sup> and interpreted in terms of transport mediated by defect-type

topological objects (Fermi-liquid droplets) in the WS phase.<sup>16</sup>

In the presence of pinning, the MR data suggests the asymptotic form of the wave function  $\psi(r) \sim \exp(r/\xi)$ , where  $\xi \approx a_B^*$ . However, the interplay of confinement arising from the magnetic potential and disorder pinning is expected to be critical in determining  $\psi(r)$ , with disorder pinning dominating at low  $B_\perp$ . This is expected to result in the upper cutoff  $B_c$  that decreases with decreasing disorder, as observed experimentally. The intricate interplay between disorder, electron-electron interaction, and magnetic field is further illustrated by the absence of a clear  $B_\perp^2$  dependence of the MR in T46 (largest  $\delta_{\text{sp}}$ ), which could be explained by a prohibitively small  $B_c$  or the very instability of the solid phase at sufficiently low disorder. On the other hand, devices with  $\delta_{\text{sp}} \lesssim 10 \text{ nm}$  showed inhomogeneity driven Coulomb-blockade oscillations in the localized regime, making the investigation of such a charge-correlated state impossible. A quantitative understanding of the scale of  $B_c$ , as well as the specific spatial structure of the ground state in the intermediate disorder regime, will require further investigations, which are presently in progress.

- 
- <sup>1</sup>B. Tanatar and D. M. Ceperley, Phys. Rev. B **39**, 5005 (1989); A. G. Eguluz, A. A. Maradudin, and R. J. Elliott, *ibid.* **27**, 4933 (1983); A. A. Koulakov, M. M. Fogler, and B. I. Shklovskii, Phys. Rev. Lett. **76**, 499 (1996).
- <sup>2</sup>J. S. Thakur and D. Neilson, Phys. Rev. B **54**, 7674 (1996); A. A. Slutskin, V. V. Slavin, and H. A. Kovtun, *ibid.* **61**, 14184 (2000); G. Benenti, X. Waintal, and J.-L. Pichard, Phys. Rev. Lett. **83**, 1826 (1999); R. Jamei, S. Kivelson, and B. Spivak, *ibid.* **94**, 056805 (2005); S. T. Chui and B. Tanatar, *ibid.* **74**, 458 (1995).
- <sup>3</sup>H. W. Jiang, R. L. Willett, H. L. Stormer, D. C. Tsui, L. N. Pfeiffer, and K. W. West, Phys. Rev. Lett. **65**, 633 (1990); V. J. Goldman, M. Santos, M. Shayegan, and J. E. Cunningham, *ibid.* **65**, 2189 (1990); H. C. Manoharan, Y. W. Suen, M. B. Santos, and M. Shayegan, *ibid.* **77**, 1813 (1996); J. Yoon, C. C. Li, D. Shahar, D. C. Tsui, and M. Shayegan, *ibid.* **82**, 1744 (1999).
- <sup>4</sup>P. D. Ye, L. W. Engel, D. C. Tsui, R. M. Lewis, L. N. Pfeiffer, and K. West, Phys. Rev. Lett. **89**, 176802 (2002); Y. Chen, R. M. Lewis, L. W. Engel, D. C. Tsui, P. D. Ye, L. N. Pfeiffer, and K. West, *ibid.* **91**, 016801 (2003).
- <sup>5</sup>A. A. Shashkin, V. T. Dolgoplov, G. V. Kravchenko, M. Wendel, R. Schuster, J. P. Kotthaus, R. J. Haug, K. von Klitzing, K. Ploog, H. Nickel, and W. Schlapp, Phys. Rev. Lett. **73**, 3141 (1994); Y. Meir, *ibid.* **83**, 3506 (1999); S. Das Sarma, M. P. Lilly, E. H. Hwang, L. N. Pfeiffer, K. W. West, and J. L. Reno, *ibid.* **94**, 136401 (2005).
- <sup>6</sup>A. L. Efros, Solid State Commun. **65**, 1281 (1988); A. L. Efros, F. G. Pikus, and V. G. Burnett, Phys. Rev. B **47**, 2233 (1993).
- <sup>7</sup>I. M. Ruzin, S. Marianer, and B. I. Shklovskii, Phys. Rev. B **46**, 3999 (1992).
- <sup>8</sup>S. T. Chui, J. Phys.: Condens. Matter **5**, L405 (1993).
- <sup>9</sup>E. Buks, M. Heiblum, and H. Shtrikman, Phys. Rev. B **49**, 14790 (1994); M. Stopa, *ibid.* **53**, 9595 (1996).
- <sup>10</sup>A. Ghosh, M. Pepper, H. E. Beere, and D. A. Ritchie, Phys. Rev. B **70**, 233309 (2004).
- <sup>11</sup>B. I. Shklovskii, Fiz. Tekh. Poluprovodn. (S.-Peterburg) **17**, 2055 (1983) [Sov. Phys. Semicond. **17**, 1311 (1983)]; B. I. Shklovskii and A. L. Efros, in *Electronic Properties of Doped Semiconductors*, Springer Series in Solid-State Sciences Vol. 45 (Springer, Berlin, 1984).
- <sup>12</sup>A. K. Savchenko, V. V. Kuznetsov, A. Woolfe, D. R. Mace, M. Pepper, D. A. Ritchie, and G. A. C. Jones, Phys. Rev. B **52**, R17021 (1995).
- <sup>13</sup>G. Timp and A. B. Fowler, Phys. Rev. B **33**, 4392 (1986).
- <sup>14</sup>S. I. Khondaker, I. S. Shlimak, J. T. Nicholls, M. Pepper, and D. A. Ritchie, Phys. Rev. B **59**, 4580 (1999); W. Mason, S. V. Kravchenko, G. E. Bowker, and J. E. Furneaux, *ibid.* **52**, 7857 (1995).
- <sup>15</sup>A. F. Andreev and I. M. Lifshitz, Zh. Eksp. Teor. Fiz. **56**, 2057 (1969) [Sov. Phys. JETP **29**, 1107 (1969)].
- <sup>16</sup>B. Spivak, Phys. Rev. B **67**, 125205 (2003).
- <sup>17</sup>G. Katomeris, F. Selva, and J.-L. Pichard, Eur. Phys. J. B **31**, 401 (2003); **33**, 87 (2003).
- <sup>18</sup>H. Noh, M. P. Lilly, D. C. Tsui, J. A. Simmons, L. N. Pfeiffer, and K. W. West, Phys. Rev. B **68**, 241308(R) (2003).